Manuscript of the article: Bányai, L., Mentes, Gy., Újvári, G., Kovács, M., Czap, Z., Gribovszki, K., Papp, G. Recurrent landsliding of a high bank at Dunaszekcső, Hungary: Geodetic deformation monitoring and finite element modeling**.**

Appeared in: Geomorphology, 2014, Volume 210, 1 April 2014, pp. 1-13. ISSN: 0169-555X

Publisher's version:

http://dx.doi.org/10.1016/j.geomorph.2013.11.032

Recurrent landsliding of a high bank at Dunaszekcső, Hungary: geodetic deformation monitoring and finite element modeling

László Bányai[a*], Gyula Mentes[a], Gábor Újvári[a], Miklós Kovács[b], Zoltán Czap[b], Katalin Gribovszki[a], Gábor Papp[a]

[a]Geodetic and Geophysical Institute of the Research Centre for Astronomy and Earth Sciences, Hungarian Academy of Sciences, Csatkai E. u. 6–8., H–9400 Sopron, Hungary
[b]Department of Geotechnics, Budapest University of Technology and Economics, Műegyetem rakpart 3, H–1111 Budapest, Hungary

*Corresponding author e–mail address (L. Bányai): banyai.laszlo@csfk.mta.hu

Abstract

Five years of geodetic monitoring data are processed to evaluate recurrent sliding at Dunaszekcső, which are characteristic geomorphological processes affecting the high banks of the Middle Danube valley in Hungary. The integrated geodetic observations provide accurate three dimensional coordinate time series, and these data are used to calculate the kinematic features of point movements and rigid body behavior of point blocks. Additional datasets are borehole tiltmeter and hydrological recordings of the Danube and soil water wells. These data, together with two dimensional final element analyses, are utilized to gain a better understanding of the physical, soil mechanical background and stability features of the high bank. Here we show that the main trigger of movements appears to be the changing groundwater levels, which have an effect an order of magnitude higher than that of river water level changes. Varying displacement rates of the sliding blocks are interpreted as having been caused by basal pore water pressure changes originating from shear zone volume changes, floods of the River Danube through later seepage and rain infiltration. Both data and modeling point to the complex nature of bank sliding at Dunaszekcső. Some features imply that the movements are rotational, some reveal slumping. By contrast, all available observational and modeling data point to the retrogressive development of the high bank at Dunaszekcső. Regarding mitigation, the detailed analysis of three basic parameters (the direction of displacement vectors, tilting, and the acceleration component of the kinematic function) is suggested because these parameters indicate the zone where the largest lateral displacements can be expected and indicate the advent of the rapid movement phase of sliding that affect high banks along the River Danube.

Keywords: River Danube; Groundwater; Bank failure; Tilting; Kinematic and dynamic evolution

1. Introduction

Mass movements are considered the major geomorphic processes that govern the morphological evolution of high banks along the River Danube on both shorter and longer timescales. In Hungary abrupt and disastrous landslides along the river were documented and their possible mechanisms were explained from geomorphic–hydrogeological point of view in the last century (e.g. Domján, 1952; Kézdi, 1970; Horváth and Scheuer, 1976; Pécsi and Scheuer, 1979; Pécsi et al., 1979; Scheuer, 1979). Active sliding phases commenced owing to the likely interplay of high water stands of the Danube, increased precipitation input and anthropogenic activity (Juhász, 1999; Kleb and Schweitzer, 2001; Szabó, 2003; Kraft, 2005). Such sliding events also occurred during the Medieval and Roman times and a rate of bluff retreat of 5–15 m per 100 years over the last 2,000 years was estimated (Lóczy et al., 1989, 2012). Previously, the bank failures were described after the main sliding phase and as yet only one real observational record is available from Hungary which includes deformation monitoring data from close to the initiation to the main phase of a landslide (Újvári et al., 2009). The morphological evolution of bluffs, however, are affected and ultimately defined by a succession of smaller–larger sliding events and to this end relatively little is known about the high bank deformations even on the short term (some years).

In 2008, a large landslide occurred at Dunaszekcső (Újvári et al., 2009) and during the subsequent years the movements spread towards the south (Fig. 1), thereby threatening numerous houses, private properties and infrastructures (Bugya et al., 2011; Mentes et al., 2012). GPS measurements and precise leveling campaigns were commenced in 2007 and these datasets were complemented with continuous tilt recordings. Subsequently, the monitoring network was extended towards the south and the 3D deformations were measured by a combination of GPS, leveling and total station instruments (Bányai, 2013). In this study, we address some basic issues of the dynamic evolution of bluffs using the 5–year records of geodetic deformation monitoring (2007–2012), hydrological data and finite element modeling of the high bank at Dunaszekcső. These questions include: 1) what are the main triggers of landsliding, 2) what are the main kinematic and dynamic characteristics of the bank failures, 3) whether a stable, displacement–free equilibrium state between the main sliding phases (dormant phases) exits, i.e. what happens to the sliding blocks after the main phases, and 4) how the measured and calculated parameters of the deformation monitoring may help in taking the appropriate mitigation measures before the main sliding events. By answering these questions we offer a synthesis of bank failure mechanisms at Dunaszekcső and a deeper understanding of the dynamic evolution of high banks along the River Danube.

2. Study area and methodology

2.1. Study area and the geodetic monitoring network

The study area is located in south Hungary at the village of Dunaszekcső, close to the Croatian border (inset of Fig. 1). The basement formations at Dunaszekcső are Triassic–Jurassic limestones located at 200–250 m below the surface (Szederkényi, 1964; Urbancsek, 1977; Moyzes and Scheuer, 1978; Hegedűs et al., 2008). These basement rocks are covered by clayey and sandy sediments formed in the Pannonian s.l. epoch (equivalent to the Upper Miocene and the Pliocene, 12.6 to ~2.6–2.4 Ma; Rónai, 1985) that can be found below about 70 m deep under the southern monitoring network (SMN, Vár Hill, Fig. 1) according to borehole data (Moyzes and Scheuer, 1978; Pécsi et al.,1979). The uppermost 70 m of the sediment sequence are sandy and clayey loess layers with brown to red fossil soils accumulated during the Pleistocene.

The bluff reaches its highest point (142 m above Baltic Sea level) at SMN where the southern and southernmost parts of the moving blocks are located (SB, SMB, Fig. 1). The floodplain of the Danube is very narrow or missing below SMN and northern monitoring network (NMN, Szent János Hill, Fig. 1). The bluff consists of a 20–30 m high vertical loess wall above the 10–20 m high slopes that consist of reworked loess from past landslides and fluvial mud, sand and gravel deposits of the Danube. The slopes were intensively undercut by the river during each flood event (Moyzes and Scheuer, 1978; Kraft, 2005).

The younger loess series on top is prone to collapse, while the older loess below is much more compact (Moyzes and Scheuer, 1978; Scheuer, 1979). The density of the younger loess deposits is around 1.6 g cm^{-3} (Papp, 2009), but that of the older loess series and the intercalated paleosols is between 2.0–2.1 g cm^{-3}, and that of the Pannonian clays and sands reaches 2.16 g cm^{-3} (Hegedűs, et al., 2008). The ground water recharged from percolated rainfall and the Lánka Stream resides in the lower part of the young and more porous loess deposits. Because of the sucking effect of the Danube (Moyzes and Scheuer, 1978), ground water flows to the South–East.

Field observations show the development of tension cracks in the loess complex parallel as well as perpendicular to the channel of the Danube, indicating reduced rock strength. The vertical cracks are clearly visible on the roof of the Töröklyuk Cave (Kraft, 2005, Újvári et al., 2009), a unique large natural cavity under northern moving block (NB, Fig. 1). Cracking was probably induced by both previous sliding events and recent slumping. Recent tectonic movements may also have influenced this process because tension cracks have also appeared in the apparently intact part of the slope 150–200 m southwards from SB.

The geographical and geomorphological settings of the study area are shown in the oblique aerial photo of Fig. 1, taken in 2008. Scarps and moving blocks of previous sliding events can easily be recognized in this image together with the northern and southern parts of the geodetic monitoring network (NMN and SMN, respectively). At the beginning of observations in 2007, four reinforced concrete pillars were established and used as a reference network (for further details see Újvári et al., 2009). Later on, another reinforced concrete pillar was built and involved in the deformation measurements, as part of the reference network. GPS baselines and tilts of the pillars were measured to check their stability and three pillars located closer to the sliding zone were used to determine baselines between the pillars and the smaller benchmarks constituting the monitoring network in the zone of active sliding (Fig. 2).

After the main sliding event (12.02.2008), the quality of GPS measurements became very poor on the subsided blocks as the GPS receivers could not record the signal of some GPS satellites due to the new terrain configuration (high vertical walls). To solve this problem, new benchmark points were established on the top of the high bank along the scarps developed in February 2008, and total station measurements were also integrated in the deformation monitoring (Bányai, 2013). Furthermore, the geodetic monitoring network has been extended towards the south because the southward spread of landsliding was expected (Fig. 2).

Regarding the three–dimensional adjustment of integrated geodetic observations in the WGS–84 coordinate system (used by GNSS techniques), a new adjustment procedure was developed (Bányai, 2013). All the data were re–adjusted so that the coordinate changes of the pillars were minimized in a least–squares sense with respect to the coordinates adapted in the first (initial) epoch. Results show that the adjusted coordinate components can be characterized by an accuracy of 2–3 mm and the pillars fulfill the stability requirements. Basic results used in this paper are the Cartesian coordinate time series of the monitoring points and the local topocentric coordinate changes (North, East and Up) determined with respect to the first measurement epoch.

2.2. Kinematic and dynamic analysis of benchmark points

The kinematic behavior of individual benchmark points can be described by the least–square fit of the known kinematic function

$$s(t) = s_0 + v_0(t - t_0) + \frac{1}{2}a(t - t_0)^2 \quad (1)$$

where $s(t)$ is the investigated coordinate component at the time t, s_0 is the starting value and v_0 is the instantaneous velocity at the arbitrarily chosen reference epoch t_0 , a is a constant acceleration in the investigated time interval, s_0, v_0, and a are the unknowns of the fit.
During the presented computations, the measured vertical (Up) time series are divided into properly chosen intervals with the starting epoch as reference (i.e., s_0 and v_0 is referred to t_0). Visual inspections and test computations can be used to choose the proper time intervals. Values, to connect the neighboring intervals, can be calculated in two different ways: a) intersection of the functions is constrained between the two neighboring intervals (where the function values are equal), and b) the same expect that first derivative of the two functions should also be equal (smooth junction). A third possibility is when the functions defined for the two neighboring intervals have no connections (discontinuity, ramp).

Inversion of the investigated time series into velocities and accelerations allows the interpretation of processes in terms of Newtonian dynamics. Significant variations in acceleration indicate changes of resulting forces, and significant velocities imply constant resulting forces. In the equilibrium state the sum of acting forces is zero and there are no movements.

Velocity and/or acceleration dominance can be measured by the t–test, i.e. ratio of the estimated components and their standard deviations estimated by least–squares adjustment. Originally, this test is designed and used to statistically investigate whether the estimated values are significantly different from zero if measurement noise is present. If both the velocity and acceleration are equally significant in a given interval, then their impact on the function value in unit time can be taken into account in assessing the dominance of velocity and/or acceleration.

One version of the dynamic Kalman–filter was also implemented. Contrary to (1) it is allowed that a can change from epoch to epoch, therefore the state vector of the process is composed of s_i , v_i and a_i triplets referring to the i–th epoch t_i (Teunissen, 2001; Strang and Borre, 1997). Using the starting values variations of the triplet can be extrapolated for the next epoch. Difference between the extrapolated and measured function values is used to update all three components of the triplet from epoch to epoch. Consequently the Kalman–filter indicates changes in accelerations that can be used to identify intervals of similar characteristics.

2.3. Rigid translations, rotations and tilts of moving blocks

Supposing that the group of points behaves as rigid bodies, their characteristics can be investigated by seven parameter similarity transformation:

$$\begin{bmatrix} N_i \\ E_i \\ U_i \end{bmatrix} = \begin{bmatrix} \Delta_N \\ \Delta_E \\ \Delta_U \end{bmatrix} + \lambda\ R_N(\alpha)\, R_E(\beta)\, R_U(\gamma) \begin{bmatrix} N_0 \\ E_0 \\ U_0 \end{bmatrix}, \quad (2)$$

where the subscripts 0 and i refer to the reference and the investigated epochs respectively, Δ_N, Δ_E and Δ_U are the rigid body translations, λ is the scale parameter, α, β and γ are the finite rotations about the local North, East and Up axes and R_N, R_E and R_U are the rotation

matrices. The translations, rotations and scale parameters can also be estimated by the least–squares adjustment, if at least three benchmark points are available and they are not located along a straight line (Závoti, 2012). The geometric interpretation of translations and rotation about the vertical (Up) axe is evident: positive rotation ($+\gamma$) is clockwise (from north to east). Rotations α and β can be interpreted as the tilt of the horizontal plane attached to the rigid body in the reference epoch:

$$N_\tau = \beta \,, \tag{3}$$

$$E_\tau = -\alpha \,, \tag{4}$$

$$b = \tan(N_\tau) \,, \tag{5}$$

$$c = \tan(E_\tau) \,, \tag{6}$$

$$\tau = \tan^{-1}(\sqrt{c^2 + b^2}) \,, \tag{7}$$

$$A_\tau = \tan^{-1}(c/b) \,, \tag{8}$$

where N_τ and E_τ are the North and East tilt components, $[b\ c\ 1]$ is a normal vector of the tilted plane, τ is the total (or maximum) tilt and A_τ is its azimuth. The parameters N_τ and E_τ can be measured directly by the borehole tiltmeters at one individual point.

2.4. Tiltmeters and hydrological recordings

Two dual–axis borehole tiltmeters (Model 722A, Applied Geomechanics Inc., USA) were applied for continuous tilt registrations (Figs. 1 and 2). The positive tiltmeter axes were oriented to the East and North directions, respectively. Temporal changes of the groundwater level were observed in two wells, one of them (W1) is located ca. 100 m west of the southern sliding block, while W2 is approximately 200 m south of W1 at a slightly lower elevation. Both tilt and ground water level data are sampled hourly and water level values are given above the Baltic Sea level. Data of daily water level (*DWL*) of the River Danube have been downloaded from the publicly available website of the Directorate of Water Management (www.vizugy.hu, last accessed: 10 May 2013). Daily averages of tilt and ground water data were calculated for a comparison with water levels of the Danube.

While tiltmeter T1 has been recording continuously since November 2007, tiltmeter T2 must have been re–installed after the main sliding event in February 2008. Tilt records of T2 are available from Augustus 2010, while ground water level data are from September 2010. Because of these facts and since a detailed analysis of the tilt and water level datasets for the period of November 2007 to February 2008 is given in Újvári et al. (2009), the period from 01.02.2010 to 27.02.2013 is investigated here.

Correlations between the individual tilt components and water levels are investigated by Pearson correlation:

$$r = \frac{1}{n-1}\sum_{i=1}^{n}\left(\frac{X_i-\mu_X}{\sigma_X}\right)\left(\frac{Y_i-\mu_Y}{\sigma_Y}\right), \tag{9}$$

where r is a correlation coefficient, X is the investigated water level, Y is the investigated tilt component, μ is a sample mean, σ is a sample standard deviation and n is a number of data.

The multiple variable linear regressions (MVR) of the investigated tilt component (Y) with respect to the water plane, defined by the data of W1 ($DW1$), data of W2 ($DW2$ and DWL data, are calculated by the equation:

$$Y = r_0 + r_1\, DW1 + r_2\, DW2 + r_3\, DWL \,, \tag{10}$$

where r_0 is a constant tilt, r_1, r_2 and r_3 are the regression coefficients or admittances, which can also be estimated by least–squares adjustment.

2.5. Finite element modeling

To better understand the physical/soil mechanical background of the sliding of the high bank at Dunaszekcső, a two dimensional analysis of deformation and stability was performed using the finite element package Plaxis 2D used in soil mechanics. For the modeling of the failure mechanism the Mohr–Coulomb material model and various material properties (Table 1) have been used. The geometric model was based on a cross–section and the geological/morphological data given in Újvári et al. (2009) reflecting conditions of the high bank before the main event (12.02.2008). All of the individual loess, fossil soil, and clay layers were defined by using triangles (15 nodes) and interface (boundary layer) elements (10 nodes). Possible effects of tension cracks were simulated by applying an anisotropic layer in the upper part of the sediment sequence. Another scenario was also tested, when a soft, plastic clayey layer evolves within the Plio–Pleistocene red clays due to excess water causing the slumping of more rigid blocks overlying it. This was done by increasing the shear strength of the uppermost two loess layers from 1 to 1.35, while leaving that of the third, clayey layer unchanged. The effect of anisotropy has also been tested in this model configuration. As a final step in the simulations, strength parameters of the soil were successively reduced until failure of the structure occurred.

3. Results

3.1. Coordinate time series

Six representative topocentric time series for the different blocks are summarized in Fig. 3. The vertical displacements of point 3003 are similar to that of point 1002 (given in Fig. 3). After the main sliding these points were still subsiding on 26.02.2008, later they uplifted and after reaching a maximum height, they were approaching their initial elevations. In fact, they are the nearest points to the scarp. The vertical characteristics of points 3000–3002 and 3004 resemble the point 1003 (given in Fig. 3). Subsequent to the main sliding event these points started uplifting and after reaching a maximum in height, these points also returned to their original elevation.

Points placed on the southern and northern moving blocks showed rapid subsidence before the main sliding phase (from September 2007 to February 2008). Otherwise, 3D displacements of points 1000, 1006, 2003 and 4002 exhibit similar patterns from 2009 onwards. All these points demonstrate a strong eastern horizontal component in their movements (i.e. towards the Danube River, Fig. 4) and even the magnitudes of the subsidence of 1000, 1006, and 2003 are in the same range (Fig. 3). This observation highlights that the southern moving block moves at a similar pace in vertical sense as the southernmost block (1000, 1001 and 1004–1006), which has been affected by sliding more recently. At the same time, 4002 experienced slower vertical displacement and this is true for other points on the northern moving block, implying a less rapid subsidence of this block. In addition, it is also clearly visible in Fig. 3 that the displacements (e.g. vertical) can be characterized by alternating phases of relatively slow and more rapid movements. This observation can further be corroborated by the numerical investigations, since changes in the velocities and accelerations are regarded as good numerical indicators to define intervals of similar kinematic features.

Individual time intervals (Table 2) were chosen by visual inspection and using a Kalman–filter. The results of kinematic calculations are summarized in Tables 3–5.

It is clearly seen in Fig. 3 that the vertical movements slowed down from late spring to early summer in 2010 and also in 2012. Considering the individual intervals, Ia (Table 2) is dominated by large negative velocities leading to very rapid subsidence (4 to 9 m within 12 hours) in 12.02.2008 and indicating the effects of constant forces. After this main event, the sliding blocks showed quite similar movements to each other. For the northern block, negative

velocities with small positive accelerations are dominant, excluding the interval IV, where negative velocities are coupled with significant negative accelerations, indicating the increase of acting forces. During intervals V and VI, the accelerations are positive again indicating the decrease of acting forces.
Movements of the southern sliding block resemble those of the northern, but with larger negative velocities. Also the negative accelerations have already been significant in the interval IIIa. For point 2004, both of the components v_0 and a are equally significant, but negative accelerations led to more significant subsidence during unit time.
On the southernmost sliding block, points 1000 and 1001 behaved in a unique way. For the interval Ib these benchmark points exhibited practically zero velocities and minor negative accelerations. This holds true for the subsequent interval (II), but the negative accelerations are even smaller. For point 1000, velocities became significant in the intervals IIIb, IV, V, and VI, with increasingly negative accelerations in the first three intervals. For the rest of benchmark points on the southernmost block, negative accelerations are significant in intervals IIIa and IV. These data refer to the increase of acting forces which ultimately led to the initiation of landsliding on the southernmost part of the Vár Hill.
Estimated rigid body translation, rotation and tilt parameters of the three sliding blocks are given in Tables 6–8. Tilt curves are plotted in Fig. 5 together with the available tilts recorded by borehole tiltmeters T1 and T2. For the comparison of block rotation and point tilting the measured data of T1 tiltmeter and estimated tilts of block (defined by point group of 400, 1002 and 1003), are also plotted in Fig. 5. They are placed near to each other and this area is regarded as the stable part of the network. Despite the minor coordinate changes and tilts, the agreement is excellent demonstrating the feasibility of the two different techniques.
While the tendency of surface tilts is similar on the northern block both before and after the main event, magnitudes of tilts are smaller after the main event. The azimuth of maximum tilts varies between –99° and –120° (western direction). During the main event, the tilt amounted only to 7.6° (azimuth –100.1°) and the average horizontal translation and subsidence to 2.5 and 9.0 m.
As for the southern block, the tilt components had opposite signs before and after the main event. The azimuth of maximum tilt ranged from +100° to +103° (eastern direction) before 12.02.2008, and varied between –60° and –70° (western direction) after the main event. On 12.02.2008, the maximum tilt was 18.9° (azimuth +84.2°), while the average horizontal displacement and subsidence amounted to 3.7 and 7.0 m.
Tilt components of the southernmost sliding block resemble those of the northern block rather than the southern block. The azimuth of maximum tilts varied between –106° and –139° (western direction) for the interval of 09.02.2009 to 25.10.2012.

3.2. Tilt records and hydrological data

Measured borehole tilts, ground water and water level data of the River Danube are shown in Fig. 6. The approximate average heights of water levels ($DW1 \approx 96.7$ m, $DW2 \approx 91.5$ m and $DWL \approx 82.5$ m) indicate the East to South–East tilt of the water table. The water level fluctuations are rather smooth in well W2, as compared to well W1, which is located at a higher position.
To investigate the effects of groundwater and river water fluctuations on tilting the available data were subjected to Pearson correlation analyses and multiple variable linear regression analysis. The calculated regression and correlation coefficients are given in Table 9. The correlation analysis demonstrates that there is no significant (0.9 or above) direct correlation between *DWL* and tilt data, and this holds true also for the groundwater level and the eastern tilt component measured by T2.

Despite this fact, the MVR yielded significant regression coefficients between the tilts and water levels. Obviously, the regression coefficients (admittances) give the amount of tilt caused by a unit change in water levels (*DW*1, *DW*2 and *DWL*). It can be seen in Table 9 that the groundwater variations measured in the upper well W1 have the strongest effect on the tilt of the southern sliding block (T2). A groundwater level increase of 1 m in well W1 causes an eastward tilt of 1028.1 μrad (admittance: 1028.1 μrad m^{-1}) and a northward tilt of 575.8 μrad of tiltmeter T2. By contrast, increasing groundwater levels in the lower well (W2) induce opposite tilt directions (e.g. a 1 m of groundwater change causes a southward tilt of 434.3 μrad). In general, the effect of water level variations of the River Danube is one order of magnitude smaller than that caused by groundwater level fluctuations. Obviously, as it can be inferred from the MVR analysis, the simultaneous falling of river water and rising of ground water levels in sediments making up the high bank play crucial role in its stability.

3.3. Finite element modeling

The main results of the numerical modeling in terms of the failure mechanisms and the shape and depth of simulated slip surfaces are displayed in Figs. 7 and 8. While the modeled vertical displacements (5–6 m, Fig. 7a) agree well with the observed subsidence after the main event (12.02.2008) (e.g. 6.4 to 7.7 m at points 2003 and 2004; Újvári et al., 2009), the model is unable to reproduce the exact location of the ruptures, i.e. the starting point of the slip surface on the top of the high bank. This may appear everywhere between 0 and 25 m from the bank's edge. At the same time, most of the modeled slip surfaces run out in front of the reworked loess debris from past landslides (Fig. 7b,c and Fig. 8). Indeed, a deformation zone with solifluction and rising of the ground was observed at the river's floodplain, confirming these simulation results. Furthermore, Fig. 8a demonstrates that various combinations of cohesion and friction angles of loess define different slip surfaces both in terms of shape and depth. Interestingly, simulations with material properties of loess types 3 and 4 produce similar slip surfaces to the situation when the slumping of rigid blocks occur over a plastic, clayey layer due to excess water (Fig. 8b).

4. Discussion

The deformation monitoring and hydrological data together with numerical modeling provide insights into the underlying physical mechanisms of bank sliding. Clearly, as the multiple variable regression analysis between tilt and hydrological data demonstrated, the groundwater level variations have a considerable effect on tilting, and in general, on bank deformations. This effect is an order of magnitude higher than that caused by the water level changes of the River Danube. Groundwater levels have been increasing at the study site since 1980s as recognized by Kraft (2011). While these levels were at 93–94 m above the Baltic sea level around 1980 (Kraft, 2011), continuous recordings in W1 reveal 96–97 m levels at present. These changing hydrological conditions resulted movements and bank retreats since the 1970s and obviously affected the physical properties of the loess, fossil soil and clayey layers making up the high bank. The hydraulic gradient forces acting on the bank lead to preferential subsurface flows from the bank towards the river, especially at low river water stages. As recognized in the field, layers at the middle and low water levels of the riverbed actively discharge bank material (mostly yellowish, loess particulates) to the river water. Obviously, this is an erosive process as it mobilizes particles from the affected layers thereby reducing their shear strengths (Fox and Wilson, 2010). At the same time, the measured uplift of points 1002, 1003 and 3000–3004 after the main sliding event may indicate the temporal movements of the bank material into the opposite direction (towards the west).

As presented in Section 3.3, the finite element modelling results point to the rotational nature of high bank sliding at Dunaszekcső. Also the single and double slider models of Karbon et al (2011) were based on this feature of the sliding. In our view, however, the nature of the bank deformations appears to be more complex: as the movements commence the sliding is rotational and subsequently it develops further as a slumping. Some of the field observations and geodetic monitoring data fit well with the rotational models, others are less consistent. While the tilts of moving blocks NB, SB and SMB (Table 6–8) fit in the rotational model (except SB between 03.10.2007 and 17.06.2009), this model is not entirely supported by the dominancy of vertical subsidence of the NB and SB blocks. Also the deformation zone with solifluction features at the river bank corroborates model results, i.e. the outcrop of the slip surfaces at the base of the loess slope (Figs. 7 and 8, Karbon et al., 2011). The major shortcoming of the presented finite element model is that it is unable to reproduce the large lateral extrusion of bank material at the landslide's toe and the resulting emergence of shallows in the river bed. The double slider block model was introduced to solve this issue (Karbon et al., 2011). This latter model, however, requires a circular, deeply penetrating sliding surface in the clayey Pliocene–Lower Pleistocene layers (and another one in the loess–paleosol strata). Boreholes drilled after the main event revealed that loess and reddish soil layers rich in carbonate concretions making up the bank material here and also reddish, clayey sediment blocks eroded from the underlying clayey–sandy layers (Pliocene–Lower Pleistocene) are present at shallow depths (0–10 m) (Kaszás and Kraft, 2009). Water content of these layers varied from 21% to 25 % and Kaszás and Kraft (2009) identified and interpreted the interface of the Middle to Late Pleistocene loess–paleosol sequence and the Pliocene–Lower Pleistocene clayey strata as the slip surface of sliding at Dunaszekcső. As admitted by Karbon et al. (2011), this is a mechanically more likely scenario and it does not necessarily require older red clay material from considerable depths (50–60 m). Another issue is that if older clayey layers had emerged from greater depths along a curved slip surface, then these layers with hydraulic conductivity significantly lower than loess would not allow the communication between loess/fossil soil strata and the river and the observed discharge of loess/soil particulates into the river. Nevertheless, this issue remains open and additional geophysical measurements at the landslide's toe (riverbank) would be needed to gain more insight into this problem.

The dynamic evolution of the high bank at Dunaszekcső is the result of the complex interplay of many factors and all the field observations and deformation measurements can be explained in a framework involving different geomorphological, geological–hydrological mechanisms and soil mechanical features. As such, previous sliding events certainly affected the high bank by creating cracks in the sediment mass that are visible on the roof of the Töröklyuk Cave (see Újvári et al., 2009), thereby reducing rock strength. Moreover, sliding activity in the past could lead to the consecutive development of more than one slip surfaces as revealed by the finite difference model of Karbon et al. (2011). These results and the field observations point to the retrogressive development of the high bank. While the lateral erosion of the Danube effectively removed the collapsed basal bank material, past slump material could impound groundwater flow towards the river leading to oversaturation of loess and soil strata. During this process, loss of matric suction, generation of positive pore water pressures and increase in unit weights of loess lead to reduced shear strength (Rinaldi and Casagli, 1999; Simon et al., 2000) and parts of the oversaturated mass slowly drifts towards the river, thereby causing slumping. Indeed, geodetic deformation data demonstrate that movements of the sliding blocks are dominated by vertical displacements (subsidence). Another crucial instrumental observation is the changing displacement rates of the moving blocks (from some mm month^{-1} to several cm month^{-1}) before and after the main event (12.02.2008) and the fact that these movements are steady, i.e. the blocks have not yet

reached an equilibrium state. In our view, one of the main factors in controlling and modulating the movements of sliding blocks is the varying basal pore water pressures. Clearly, shear zone volume changes (dilation or contraction) during slumping strongly affect basal pore water pressures thereby regulating basal Coulomb friction (Iverson, 2005). For instance, contraction of basal material results in elevated pore pressures, producing a positive feedback, namely the acceleration of block deformations. Of course, this process is affected by floods of the Danube River through later seepage (Fox and Wilson, 2010) and by rain water infiltration, but the latter process has only a restricted effect. Thus, the sliding blocks move generally slowly and with varying speeds as determined by the main first–order triggers (groundwater and river water level changes), and secondary factors (basal shear zone deformations). Obviously, the main directions of these slow block movements are influenced by sediment masses of collapsed bank materials stemming from past landslides. The interplay of the aforementioned processes in the basal shear zone will finally lead to rapid movements on the order of several meters in a day as happened on 12.02.2008. Such bank failures are expected to happen along the River Danube on the recession limb of hydrographs as demonstrated in previous studies (Domján, 1952; Karácsonyi and Scheuer, 1972; Horváth and Scheuer, 1976; Újvári et al., 2009), when the combination of the increase in pressure head, due to lateral infiltration from the river at high stages, and subsequent opposite, erosive seepage flow and reduced confining pressure of the river at low stages occurs.

5. Conclusions

Geodetic monitoring provides a wealth of information on bank deformations and a crucial issue is how the measured and calculated data can aid the planning of recommended actions to reduce, avoid or offset the adverse consequences of landsliding. By analysing our datasets and the observed bank deformations together, three important parameters emerge from the measured and calculated data: direction of displacement vectors, tilting, and the acceleration component of the kinematic functions. According to the observations, displacement vectors of the sliding blocks point towards the zone where the largest lateral displacements are expected. Before the main sliding on 12.02.2008 these vectors marked out the zone in front of the Sánc Moat, an artificial trench separating NB and SB blocks, and the bulge subsequently protruded into the river at almost the same location (Újvári et al., 2009). Once the movements started affecting the southernmost part of the Vár Hill, the horizontal movement vectors slightly rotated and now they point to an area south of the bulge formed during the main event (Fig. 4). It is that the largest lateral extrusions of bank material and deformation of the Danube River's bed will occur in this zone in the future. Another measured quantity, tilting and its direction and pace on the moving block can help in predicting the advent of the rapid movement phase, if the sliding has a rotation component (see Fig. 8 in Újvári et al., 2009; Mentes et al., 2012). Furthermore, this study reveals that parameters of the kinematic functions provide additional knowledge on the nature of movements and approximate initiation of the rapid phase. As demonstrated by the calculated kinematic parameters (Tables 3–5) and observed bank deformations, the rapid phase is approaching once the accelerations of vertical displacements result in large velocities leading to intensive subsidence.

In the time intervals Ia the velocities reached high values between –0.820 and –0.345 m y^{-1} just before the main event. Another important condition was that the affected layers were able to escape very rapidly into the riverbed of the Danube forming a bulge. The increasing but significantly smaller velocities in the SMB block, determined after the main event, may reach the necessary conditions again, or the effected layers will escape gradually for years into the Danube without intensive sliding.

According to the geodetic observations the following phases of bank movements can be distinguished. 1) Initiation of deformations: coordinate changes may be significant, but the

cracks are still invisible on the ground. 2) Cracks and ruptures are visible and the coordinate changes accelerate. 3) Significant accelerations result in very fast sliding under few hours. 4) After the mean event the sliding of sediment blocks continues for years before reaching an equilibrium state.

Acknowledgements

This study was supported by the Hungarian National Research Fund (OTKA–K 78332) and partly by the Earth System Project (TÁMOP–4.2.2.C–11/1/KONV–2012–0015). The authors are grateful for the field assistance from Attila Horváth, Frigyes Bánfi, Tibor Molnár and Ferenc Schlaffer as well as for the technical assistance from the local government at Dunaszekcső. Valuable comments made by the editor and the reviewers (Profs. Takashi Oguchi, Jan Kalvoda and Ewald Brückl) improved this paper considerably and are gratefully acknowledged.

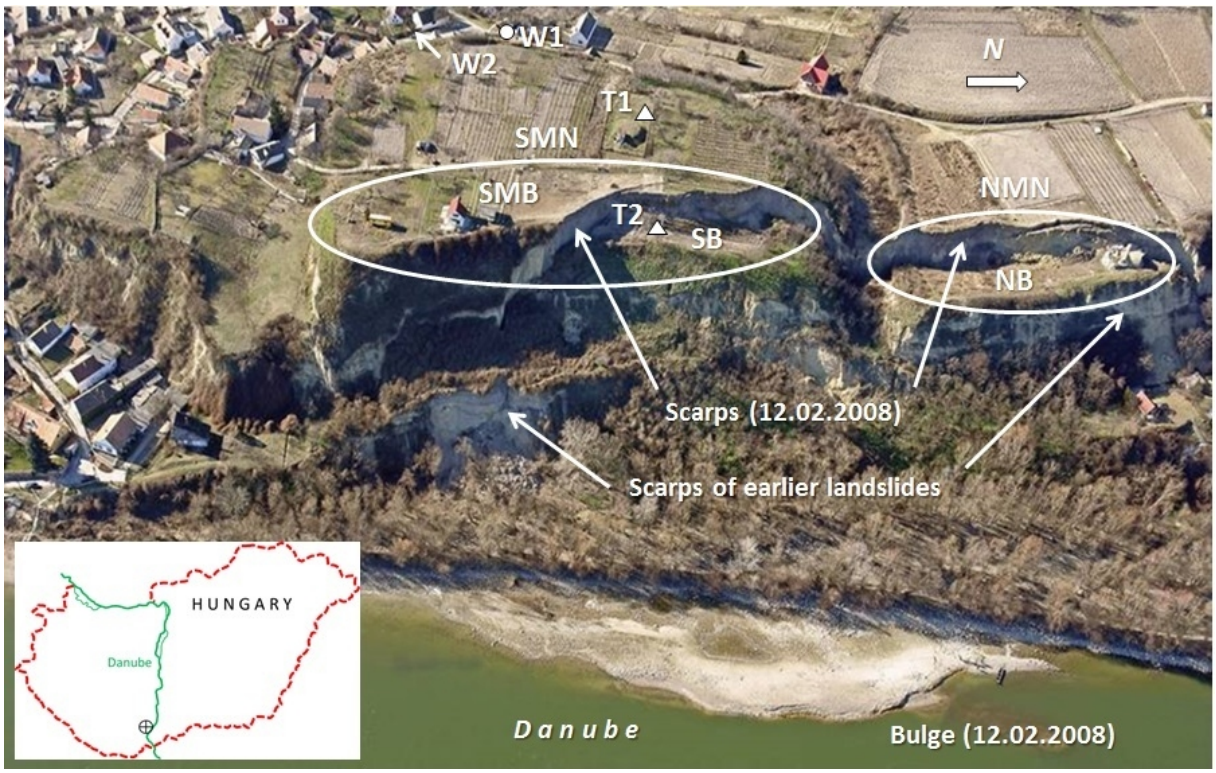

Fig. 1. Oblique aerial photo of the study area (source: László Körmendy, 17.02.2008). NB, SB, and SMB denote the northern, southern, and southernmost sliding blocks. T1 and T2 indicate the location of borehole tiltmeters, while W1 and W2 mark the groundwater wells. Ellipses with NMN at the Szent János Hill and SMN at the Vár Hill indicate the northern and southern parts of the geodetic monitoring network, which are separated by the Sánc Moat (an artificial trench). The inset map shows the location of study site.

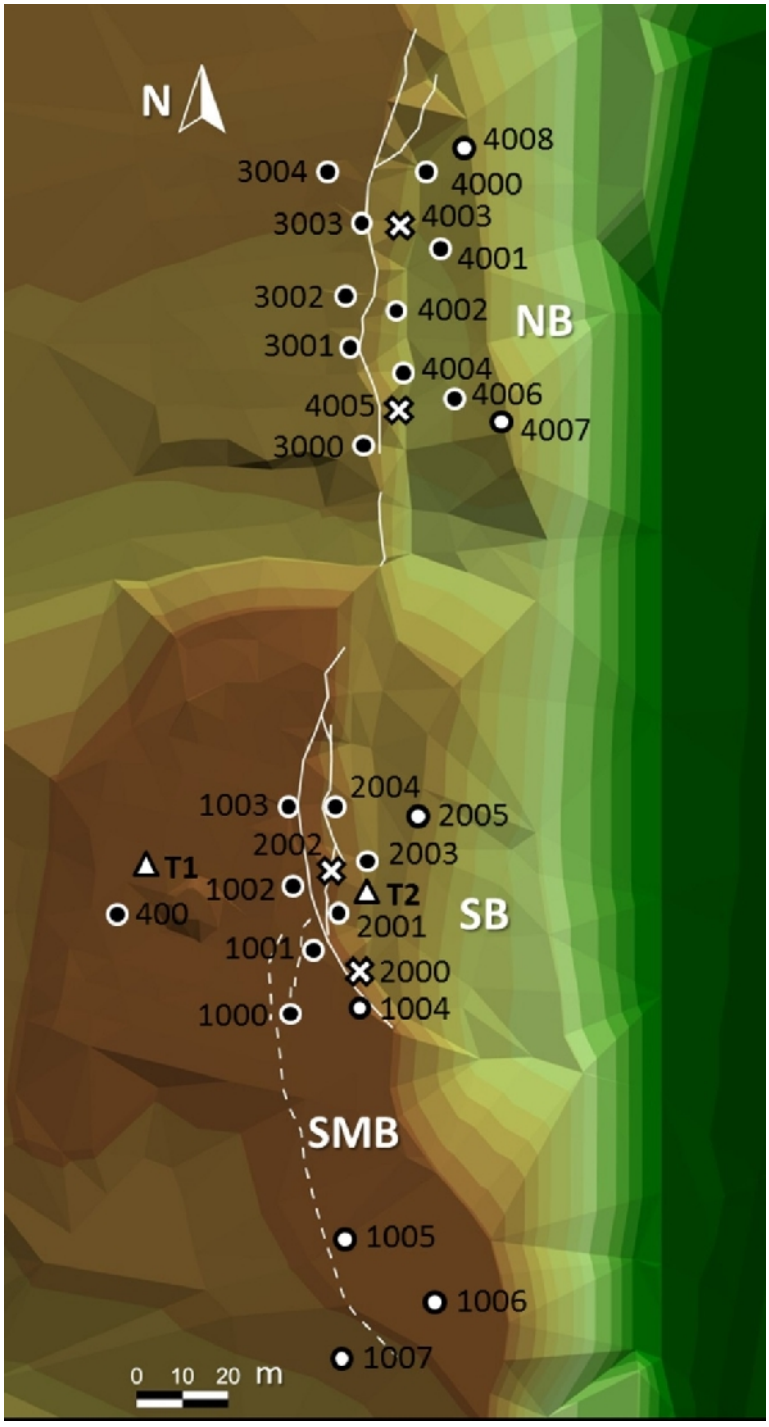

Fig. 2. Study area and the deformation monitoring network at Dunaszekcső. Isolines show the terrain after the main sliding event on 12.02.2008. Black filled circles benchmarks were established in 2007 and crosses denote points that were lost during the main sliding event. White filled circles denote new benchmarks established in 2009. The continuous white line indicates the main ruptures after 12.02.2008, and the dashed white line denotes the new rupture developed in 2010. NB (northern sliding block): 4000–4007, SB (southern sliding block): 2000–2005, SMB (southernmost sliding block): 1000, 1001 and 1004–1006.

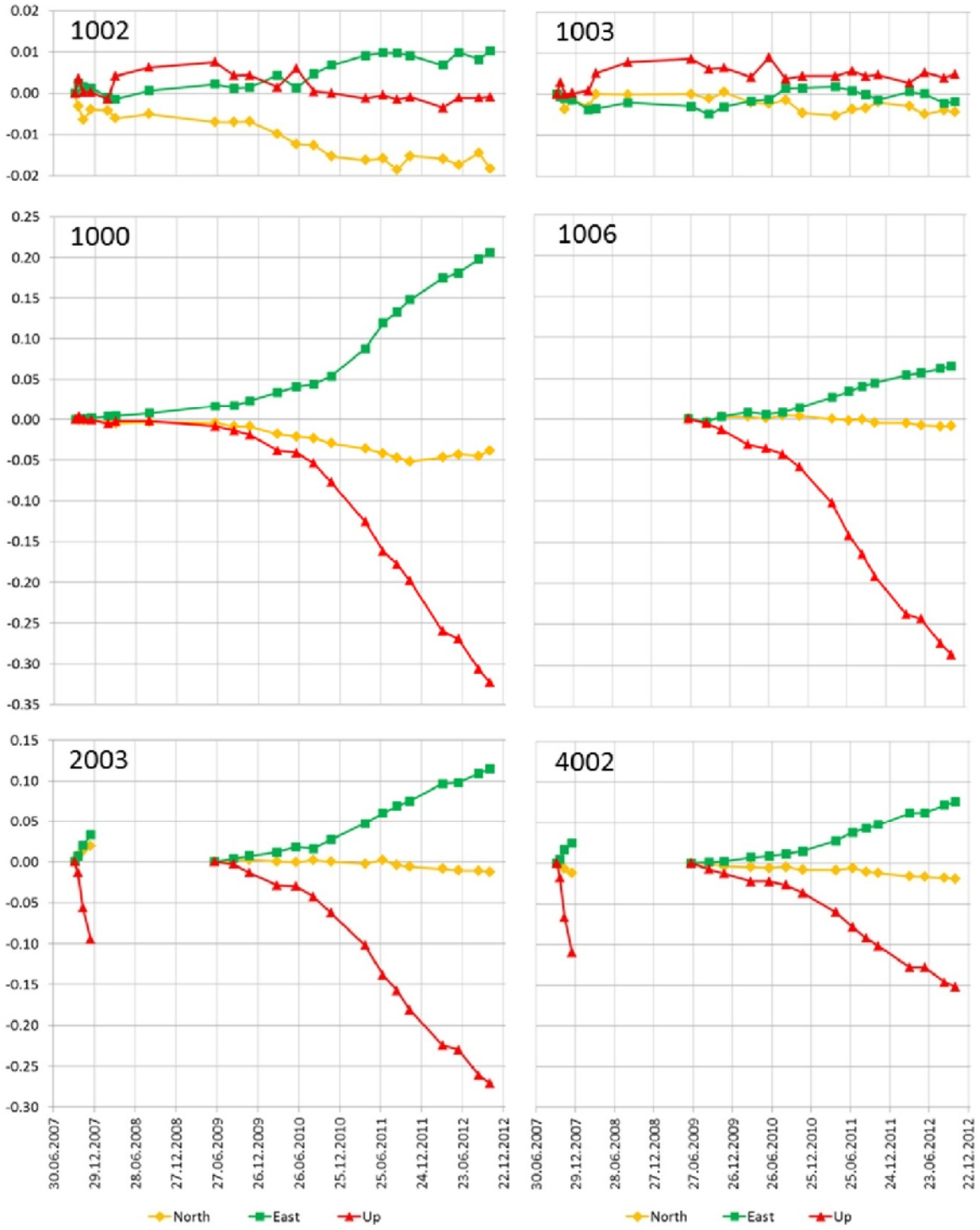

Fig. 3. Characteristic topocentric coordinate changes of some selected benchmark points (given in m). From 2009 the curves of point 2003 are shifted by –1.414, –2.481, +8.153 m, and the curves of point 4002 by +0.441, –2.693, +9.960 m in North, East and Up components to plot the curves again from zero values.

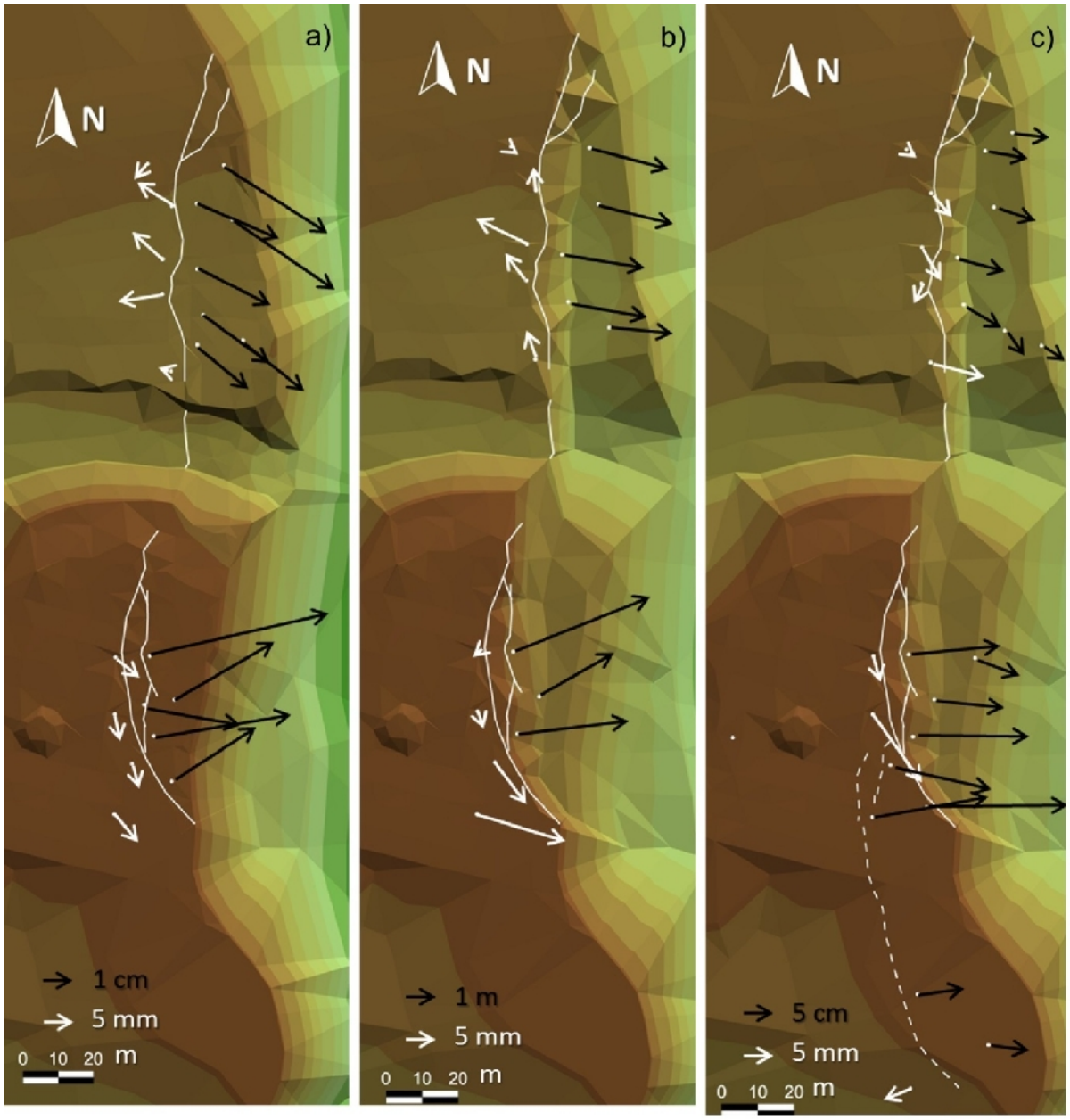

Fig. 4. Horizontal coordinate changes of benchmarks: (a) from 03.10.2007 to 13.12.2007, (b) from 13.12.2007 to 26.02.2008 and (c) from 26.02.2008 to 24.10.2012. Isolines in (a) show the terrain before 12.02.2008. White arrows show the small changes in stable areas, while black arrows show the significant changes. Note that the scales of vectors are different.

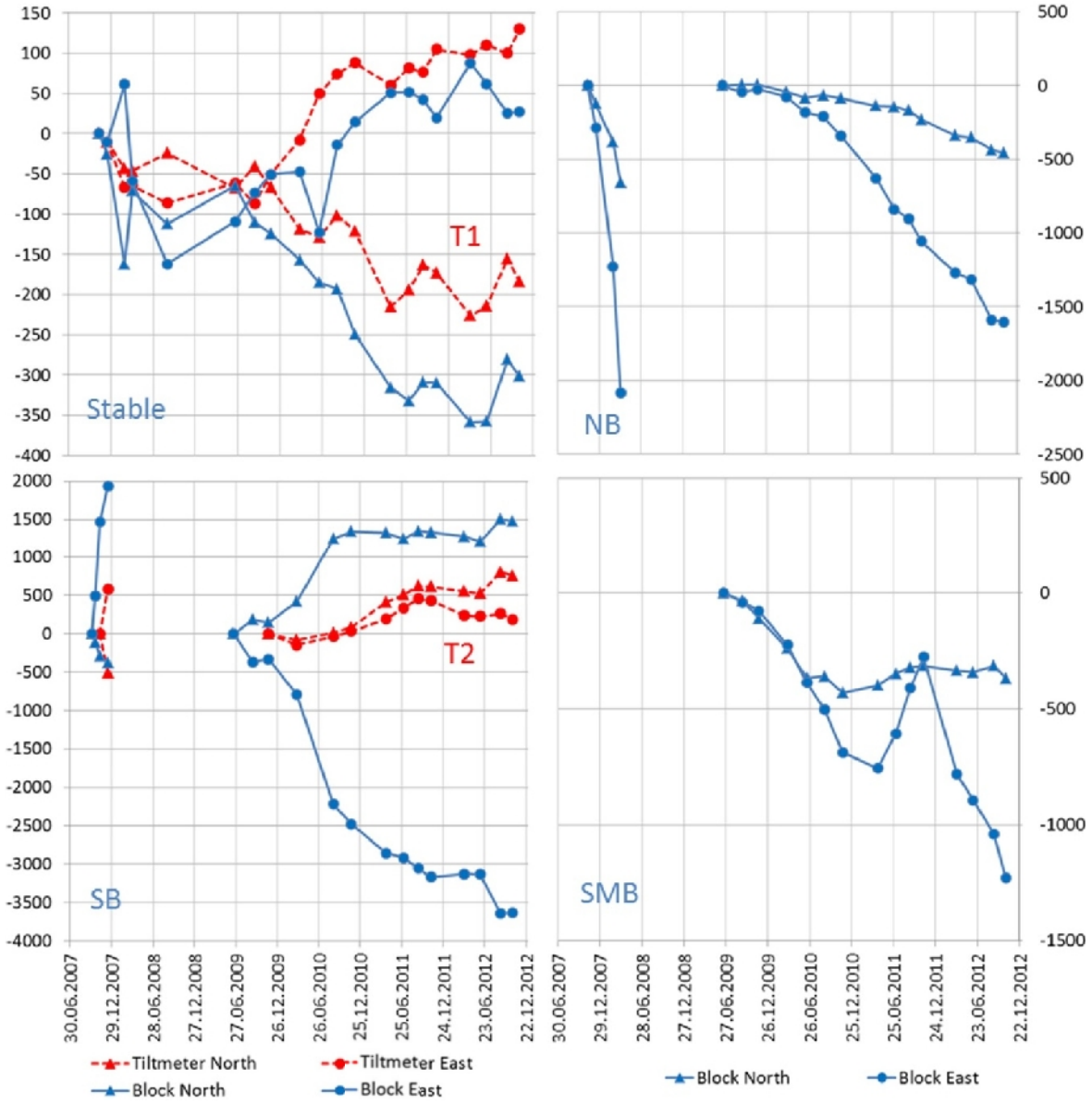

Fig. 5. Tilt curves (given in μrad) measured by borehole tiltmeters T1 and T2 (dashed lines, recorded at the reference times of geodetic observations) and estimated by block rotations (solid lines). Stable block (defined by point group of 400, 1002 and 1003), southern block (SB), northern block (NB), and southernmost sliding block (SMB).

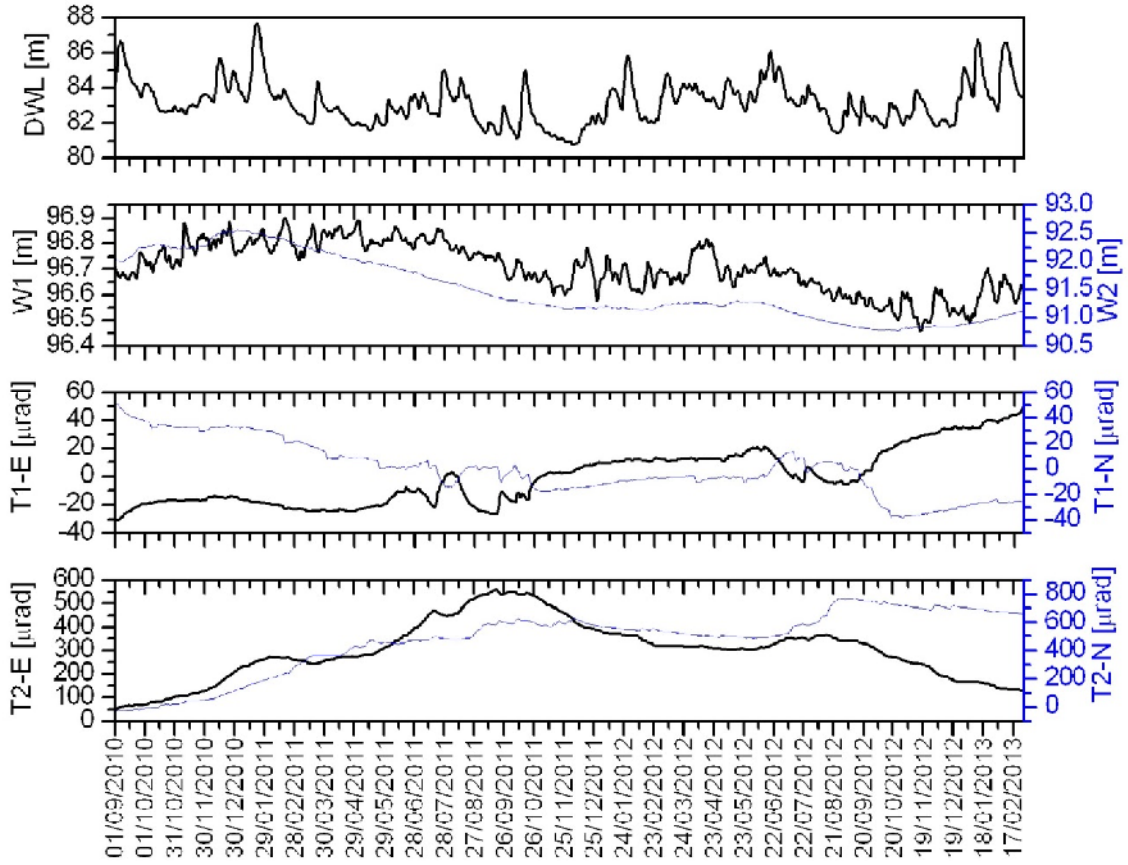

Fig. 6. Groundwater, Danube River's water level and tilt recordings for the period of 10.09.2010 to 27.02.2013. Water level of the River Danube (*DWL*) and the ground water levels measured in wells W1 and W2 are given relative to the Baltic Sea level. The North (N) and East (E) components of tiltmeters T1 and T2 are given in µrad. Increasingly positive values of eastern components (T1–E and T2–E) mean eastward tilt, while negative values indicate westward tilt. Increasing northern components (T1–N and T2–N) mean northward tilt, while negative values indicate southward tilt.

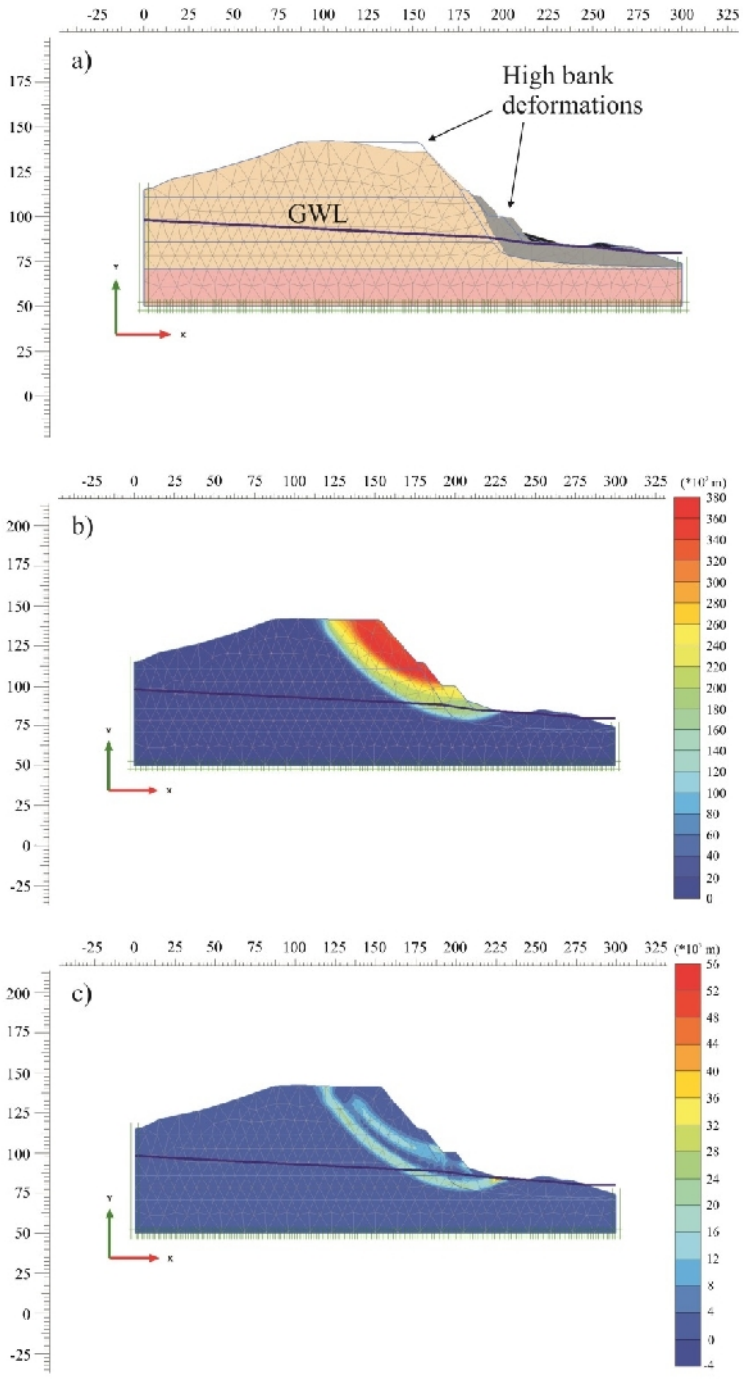

Fig. 7. Finite element modeling results: (a) the deformed mesh, (b) total displacements, and (c) total deviatoric strain. GWL is a ground water curve in the model.

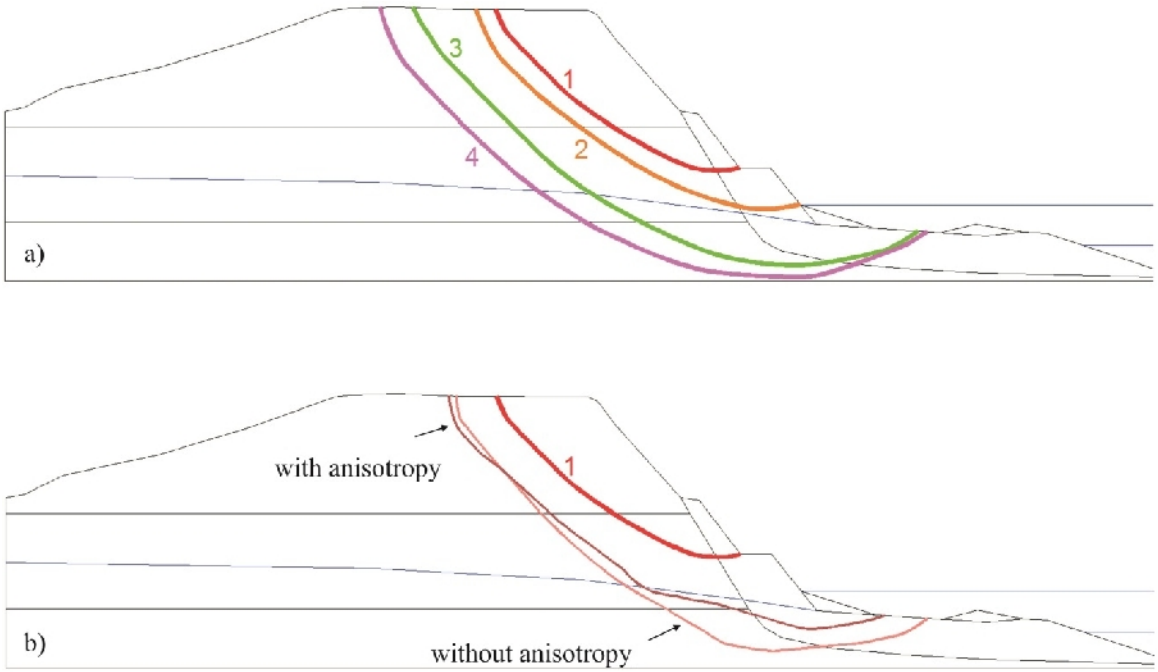

Fig. 8. Modeled slip surfaces for (a) four loess types with different physical properties and for (b) slumping of sediment blocks above a plastic clayey layer.

Table 1. Physical parameters and properties of loess and clays used in finite element modeling

Parameter	Loess				Clay
	1	2	3	4	
Modulus of elasticity (MPa)	10	10	10	10	15
Poisson ratio	0.37	0.4	0.4	0.4	0.4
Internal friction angle (°)	28.3	22.4	19.1	14.3	
Cohesion (kPa)	29.6	45.2	55.3	77.5	
Undrained shear strength (kPa)					300
Volumetric weight (kN m^{-3})	17	17	17	17	
Saturated volumetric weight (kN m^{-3})	20.6	20.6	20.6	20.6	21

Table 2. Intervals defined in kinematic calculations

Code	Interval	comments
Ia	03.10.2007 – 13.12.2007	before 12.02.2008
Ib	03.10.2007 – 26.02.2008	before 12.02.2008 (points 1000 and 1001)
II	31.03.2008 – 17.06.2009	after 12.02.2008 (points 1000 and 1001)
IIIa	17.06.2009 – 22.03.2010	after 12.02.2008
IIIb	09.09.2009 – 22.03.2010	after 12.02.2008 (points 1000 and 1001)
IV	14.06.2010 – 18.04.2011	after 12.02.2008
V	05.07.2011 – 27.03.2012	after 12.02.2008
VI	05.06.2012 – 24.10.2012	after 12.02.2008

Table 3. Kinematic parameters of benchmark points on the northern sliding block. v_0 – instantaneous velocity at the first epoch of the interval, a – constant acceleration, σ – the standard deviation, d – the Student value, Up – the measured value at the end of the interval. The dominant parameter (d_{v_0} or d_a) is given in bold.

point	interval	v_0	σ_{v_0}	d_{v_0}	a	σ_a	d_a	Up
		$(m\ y^{-1})$			$(m\ y^{-2})$			(m)
	Ia	–0.496	0.049	**10.2**	1.144	0.465	2.5	–0.072
	IIIa	–0.038	0.012	**3.3**	0.026	0.029	0.9	–8.305
4000	IV	–0.018	0.011	1.6	–0.061	0.024	**2.5**	–8.341
	V	–0.073	0.013	**5.5**	0.029	0.033	0.9	–8.406
	VI	–0.093	0.026	**3.5**	0.185	0.137	1.3	–8.428
	Ia	–0.546	0.053	**10.3**	1.159	0.506	2.3	–0.081
	IIIa	–0.041	0.013	**3.2**	0.033	0.031	1.1	–8.485
4001	IV	–0.017	0.012	1.4	–0.060	0.026	**2.3**	–8.520
	V	–0.076	0.014	**5.3**	0.029	0.036	0.8	–8.586
	VI	–0.111	0.029	**3.9**	0.268	0.149	1.8	–8.609
	Ia	–0.736	0.071	**10.4**	1.549	0.681	2.3	–0.110
	IIIa	–0.033	0.017	**2.0**	0.009	0.042	0.2	–9.983
4002	IV	–0.018	0.016	1.2	–0.063	0.035	**1.8**	–10.021
	V	–0.075	0.019	**3.9**	0.022	0.048	0.5	–10.088
	VI	–0.101	0.039	**2.6**	0.203	0.201	1.0	–10.112
4003	Ia	–0.701	0.250	**2.8**	1.343	2.397	0.6	–0.107
	Ia	–0.765	0.071	**10.8**	1.602	0.679	2.4	–0.114
	IIIa	–0.037	0.017	**2.2**	0.015	0.042	0.3	–10.204
4004	IV	–0.027	0.016	1.7	–0.067	0.035	**1.9**	–10.253
	V	–0.093	0.019	**4.8**	0.026	0.048	0.5	–10.336
	VI	–0.130	0.038	**3.4**	0.284	0.200	1.4	–10.366
4005	Ia	–0.820	0.253	**3.2**	1.653	2.425	0.7	–0.124
	Ia	–0.667	0.059	**11.3**	1.392	0.566	2.5	–0.100
	IIIa	–0.033	0.014	**2.3**	–0.002	0.035	0.0	–8.758
4006	IV	–0.022	0.013	1.7	–0.064	0.029	**2.2**	–8.805
	V	–0.086	0.016	**5.4**	0.022	0.040	0.5	–8.882
	VI	–0.100	0.032	**3.1**	0.158	0.167	0.9	–8.910
	IIIa	–0.032	0.003	**10.7**	0.007	0.007	1.0	–0.022
4007	IV	–0.009	0.003	3.3	–0.074	0.006	**12.0**	–0.057
	V	–0.076	0.003	**22.9**	0.019	0.008	2.3	–0.124
	VI	–0.095	0.007	**14.2**	0.174	0.035	5.0	–0.148
	IIIa	–0.039	0.005	**7.6**	0.034	0.013	2.7	–0.020
4008	IV	–0.018	0.005	3.7	–0.055	0.011	**5.1**	–0.054
	V	–0.064	0.006	**11.1**	0.018	0.015	1.2	–0.116
	VI	–0.082	0.012	**7.1**	0.166	0.061	2.7	–0.135

Table 4. Kinematic parameters of benchmark points on the southern sliding block. v_0 – instantaneous velocity at the first epoch of the interval, a – constant acceleration, σ – the standard deviation, d – the Student value, Up – the measured value at the end of the interval. The dominant parameter (d_{v_0} or d_a) is given in bold.

point	interval	v_0	σ_{v_0}	d_{v_0}	a	σ_a	d_a	Up
		$(m\ y^{-1})$			$(m\ y^{-2})$			(m)
2000	Ia	–0.595	0.225	**2.6**	0.851	2.156	0.4	–0.096
	Ia	–0.544	0.071	**7.6**	0.672	0.683	1.0	–0.090
	IIIa	–0.017	0.017	1.0	–0.058	0.042	**1.4**	–6.317
2001	IV	–0.049	0.016	**3.0**	–0.073	0.035	2.1	–6.387
	V	–0.122	0.019	**6.4**	0.026	0.049	0.5	–6.503
	VI	–0.136	0.039	**3.5**	0.203	0.201	1.0	–6.547
2002	Ia	–0.281	0.133	**2.1**	0.352	1.280	0.3	–0.046
	Ia	–0.594	0.076	**7.9**	0.881	0.724	1.2	–0.095
	IIIa	–0.016	0.018	0.9	–0.060	0.044	**1.4**	–8.182
2003	IV	–0.064	0.017	**3.8**	–0.052	0.038	1.4	–8.255
	V	–0.135	0.020	**6.6**	0.042	0.052	0.8	–8.377
	VI	–0.161	0.041	**3.9**	0.276	0.213	1.3	–8.424
	Ia	–0.345	0.056	**6.1**	–0.329	0.539	0.6	–0.070
	IIIa	–0.027	0.014	2.0	–0.068	0.033	2.0	–6.741
2004	IV	–0.073	0.013	**5.7**	–0.040	0.028	1.4	–6.836
	V	–0.137	0.015	**9.0**	0.061	0.038	1.6	–6.953
	VI	–0.192	0.030	**6.3**	0.389	0.159	2.4	–7.003
	IIIa	–0.012	0.008	1.6	–0.059	0.019	**3.1**	–0.026
2005	IV	–0.047	0.007	**6.4**	–0.056	0.016	3.5	–0.083
	V	–0.114	0.009	**13.1**	0.021	0.022	0.9	–0.191
	VI	–0.128	0.018	**7.3**	0.184	0.091	2.0	–0.231

Table 5. Kinematic height parameters of benchmark points on the southernmost sliding block. v_0 – instantaneous velocity at the first epoch of the interval, a – constant acceleration, σ – the standard deviation, d – the Student value, Up – the measured value at the end of the interval. The dominant parameter (d_{v_0} or d_a) is given in bold.

point	interval	v_0	σ_{v_0}	d_{v_0}	a	σ_a	d_a	Up
		$(m\ y^{-1})$			$(m\ y^{-2})$			(m)
	Ib	0.005	0.010	0.5	–0.094	0.047	**2.0**	–0.006
	II	0.004	0.003	1.3	–0.015	0.004	**3.6**	–0.009
	IIIb	–0.026	0.002	**16.1**	–0.081	0.010	8.5	–0.038
1000	IV	–0.066	0.005	**14.1**	–0.084	0.010	8.0	–0.126
	V	–0.087	0.005	**15.3**	–0.131	0.014	9.2	–0.260
	VI	–0.169	0.011	**14.9**	1.392	1.936	0.7	–0.323
	Ib	0.006	0.012	0.5	–0.086	0.057	**1.5**	–0.005
	II	0.006	0.004	1.6	–0.012	0.005	**2.4**	0.001
	IIIb	–0.013	0.002	**6.5**	–0.027	0.012	2.3	–0.013
1001	IV	–0.019	0.006	3.2	–0.139	0.013	**10.8**	–0.077
	V	–0.164	0.007	**23.5**	0.034	0.018	1.9	–0.231
	VI	–0.167	0.014	**11.9**	0.211	0.073	2.9	–0.287
	IIIa	–0.018	0.007	2.7	–0.061	0.017	**3.6**	–0.032
1004	IV	–0.044	0.006	6.9	–0.138	0.014	**9.8**	–0.120
	V	–0.169	0.008	**22.0**	0.068	0.019	3.5	–0.269
	VI	–0.162	0.015	**10.5**	0.223	0.080	2.8	–0.323
	IIIa	–0.026	0.008	3.1	–0.063	0.021	3.1	–0.038
1005	IV	–0.037	0.008	4.7	–0.137	0.017	**7.9**	–0.125
	V	–0.179	0.010	**18.9**	0.077	0.024	3.2	–0.280
	VI	–0.139	0.019	**7.3**	0.086	0.099	0.9	–0.334
	IIIa	–0.018	0.008	2.3	–0.063	0.018	**3.4**	–0.032
1006	IV	–0.026	0.007	3.7	–0.126	0.016	**8.2**	–0.102
	V	–0.161	0.008	**19.1**	0.077	0.021	3.6	–0.238
	VI	–0.135	0.017	**8.0**	0.115	0.088	1.3	–0.287

Table 6. Rigid body translations (Δ_N, Δ_E and Δ_U), horizontal rotation (γ) and tilt components (N_τ, E_τ, τ and A_τ) of the northern sliding block (NB). a) reference epoch: 03.10.2007, points: 4000–4006, b) reference epoch: 13.12.2007, points: 4000–4002, 4004 and 4006, c) reference epoch: 17.06.2009, points: 4000–4002, 4004 and 4006– 4008,* tilts are given in (°).

	epoch	Δ_N	Δ_E	Δ_U	γ	N_τ	E_τ	τ	A_τ
			(m)		(°)		(μrad)		(°)
	18.10.2007	–0.003	0.004	–0.017	0.001	–122.8	–285.9	311.2	–113.2
a)	08.11.2007	–0.009	0.016	–0.061	0.014	–383.7	–1227.2	1285.9	–107.4
	13.12.2007	–0.016	0.026	–0.101	0.022	–656.2	–2081.0	2182.1	–107.5
b)	17.06.2009	–0.473	2.479	–9.028	0.530	–1.350*	–7.575*	7.692*	–100.1
	09.09.2009	–0.002	0.001	–0.008	0.000	8.5	–44.5	45.3	–79.2
	18.11.2009	–0.002	0.003	–0.014	–0.001	7.3	–24.1	25.2	–73.1
	22.03.2010	–0.004	0.008	–0.022	–0.000	–43.8	–75.7	87.4	–120.1
	14.06.2010	–0.007	0.007	–0.023	0.004	–83.4	–182.9	201.0	–114.5
	30.08.2010	–0.005	0.008	–0.028	0.003	–65.6	–210.1	220.2	–107.3
	16.11.2010	–0.008	0.011	–0.037	0.006	–86.8	–343.1	353.9	–104.2
c)	18.04.2011	–0.008	0.020	–0.060	0.007	–137.0	–628.1	642.9	–102.3
	05.07.2011	–0.006	0.028	–0.080	0.012	–142.7	–838.9	851.0	–99.7
	06.09.2011	–0.010	0.033	–0.094	0.010	–168.5	–903.0	918.6	–100.6
	02.11.2011	–0.011	0.036	–0.103	0.012	–230.9	–1055.4	1080.4	–102.3
	27.03.2012	–0.015	0.048	–0.130	0.014	–337.1	–1267.7	1311.7	–104.9
	05.06.2012	–0.016	0.048	–0.129	0.013	–351.4	–1314.9	1361.0	–105.0
	03.09.2012	–0.019	0.054	–0.148	0.016	–436.0	–1590.5	1649.2	–105.3
	24.10.2012	–0.019	0.059	–0.153	0.018	–457.6	–1602.3	1666.3	–105.9

Table 7. Rigid body translations (Δ_N, Δ_E and Δ_U), horizontal rotation (γ) and tilt components (N_τ, E_τ, τ and A_τ) of southern block (SB), a) reference epoch: 03.10.2007, points: 2000–2004, b) reference epoch: 13.12.2007, points: 2001, 2003 and 2004, c) reference epoch: 17.06.2009, points: 2001, 2003, 2004 and 2005; * tilts are given in (°).

	epoch	Δ_N	Δ_E	Δ_U	γ	N_τ	E_τ	τ	A_τ
			(m)		(°)		(μrad)		(°)
	18.10.2007	0.004	0.008	–0.012	0.005	–112.4	489.7	502.4	103.0
a)	08.11.2007	0.009	0.026	–0.050	0.019	–289.9	1465.9	1494.3	101.2
	13.12.2007	0.014	0.041	–0.088	0.037	–379.6	1935.4	1972.3	101.1
b)	17.06.2009	1.208	3.547	–6.962	1.590	1.968*	18.822*	18.910*	84.2
	09.09.2009	0.000	0.004	–0.004	–0.014	183.0	–364.1	407.5	–63.3
	18.11.2009	0.002	0.008	–0.014	–0.013	150.4	–330.8	363.4	–65.5
	22.03.2010	0.001	0.015	–0.031	–0.016	419.7	–792.5	896.7	–62.1
	30.08.2010	0.004	0.023	–0.049	–0.013	1247.2	–2216.7	2543.5	–60.6
	16.11.2010	0.003	0.036	–0.067	–0.021	1344.2	–2474.8	2816.3	–61.4
c)	18.04.2011	–0.001	0.057	–0.105	–0.042	1326.5	–2853.1	3146.4	–65.1
	05.07.2011	0.004	0.070	–0.139	–0.057	1248.9	–2914.6	3170.9	–66.8
	06.09.2011	–0.001	0.079	–0.157	–0.054	1350.9	–3052.8	3338.3	–66.1
	02.11.2011	–0.002	0.086	–0.180	–0.070	1332.2	–3167.4	3436.1	–67.2
	27.03.2012	–0.003	0.109	–0.221	–0.073	1279.8	–3127.5	3379.2	–67.7
	05.06.2012	–0.004	0.111	–0.226	–0.075	1212.0	–3133.8	3360.0	–68.9
	03.09.2012	–0.004	0.124	–0.256	–0.089	1501.5	–3643.3	3940.6	–67.6
	24.10.2012	–0.007	0.129	–0.266	–0.095	1482.6	–3630.4	3921.4	–67.7

Table 8. Rigid body translations (Δ_N, Δ_E and Δ_U), horizontal rotation (γ) and tilt components (N_τ, E_τ, τ and A_τ) of the southernmost sliding block (SMB), c) reference epoch: 17.06.2009, points: 1000, 1001, 1004, 1005 and 1006.

	epoch	Δ_N	Δ_E	Δ_U	γ	N_τ	E_τ	τ	A_τ
			(m)		(°)		(μrad)		(°)
	09.09.2009	–0.003	–0.002	–0.006	0.004	–35.7	–41.2	54.6	–131.0
	18.11.2009	–0.002	0.004	–0.012	0.002	–110.0	–77.8	134.8	–144.7
	22.03.2010	–0.006	0.014	–0.029	0.006	–239.4	–225.4	328.8	–136.7
	14.06.2010	–0.007	0.017	–0.032	0.014	–367.0	–388.3	534.3	–133.3
	30.08.2010	–0.005	0.019	–0.042	0.010	–360.1	–502.1	617.8	–125.6
	16.11.2010	–0.010	0.029	–0.061	0.017	–431.4	–688.1	812.2	–122.1
c)	18.04.2011	–0.012	0.055	–0.108	0.032	–399.7	–756.7	855.8	–117.8
	05.07.2011	–0.012	0.075	–0.151	0.046	–349.1	–607.1	700.3	–119.9
	06.09.2011	–0.014	0.087	–0.173	0.047	–322.1	–409.8	521.2	–128.2
	02.11.2011	–0.015	0.098	–0.200	0.057	–315.3	–276.7	419.5	–138.7
	27.03.2012	–0.014	0.121	–0.254	0.071	–336.1	–782.6	851.7	–113.2
	05.06.2012	–0.012	0.125	–0.262	0.074	–342.2	–895.3	958.4	–110.9
	03.09.2012	–0.013	0.138	–0.295	0.084	–314.4	–1042.0	1088.4	–106.8
	24.10.2012	–0.011	0.145	–0.309	0.089	–369.0	–1231.1	1285.3	–106.6

Table 9. Correlation and multiple regression analyses results for the different tilt components of instruments T1 and T2, ground water levels (*DW*1 and *DW*2) and the water level of the River Danube (*DWL*).

Tilt-meter	Regression coefficients (μrad m^{-1})			Correlation coefficients		
	*DW*2	*DW*1	*DWL*	*DW*2	*DW*1	*DWL*
T1 East	-24.2	-36.0	4.4	-0.773	-0.704	0.135
T1 North	35.6	-25.7	1.0	0.859	0.639	0.228
T2 East	-208.5	1028.1	-28.4	-0.336	0.044	-0.396
T2 North	-434.3	575.8	-20.3	-0.904	-0.623	-0.298

References

Bányai, L., 2013. Three–dimensional adjustment of integrated geodetic observables in Earth–centred and Earth–fixed coordinate system. Acta Geodaetica et Geophysica Hungarica 48,163–177.

Bugya, T., Fábián, Sz.Á., Görcs, N.L., Kovács, I.P., Radvánszky, B., 2011. Surface changes on a landslide affected high bluff in Dunaszekcső (Hungary). Central European Journal of Geosciences 3, 119– 128.

Domján, J., 1952. Középdunai magaspartok csúszásai (Slides of the bluffs along the middle reach of the River Danube). Hidrológiai Közlöny 32, 416–422 (in Hungarian).

Fox, G.A., Wilson, G.V., 2010. The role of subsurface flow in hillslope and stream bank erosion: a review. Soil Science Society of America Journal 74, 717–733.

Hegedűs, E., Kovács, A.Cs., Fancsik, T., 2008. A megcsúszott dunaszekcsői löszfal aktív és passzív szeizmikus vizsgálata (Active and passive seismic investigation of the slipped loess bluff at Dunaszekcső). ResearchReportof the Eötvös Lorand Geophysical Institute, p. 20.

Horváth, Zs., Scheuer, Gy., 1976. A dunaföldvári partrogyás mérnökgeológiai vizsgálata (Engineering geological investigation of the bank collapse at Dunaföldvár). Földtani Közlöny 106, 425–440 (in Hungarian with German abstract).

Iverson, R.M., 2005. Regulation of landslide motion by dilatancy and pore pressure feedback. Journal of Geophysical Research 110, F02015, doi: 10.1029/2004JF000268.

Juhász, Á., 1999. A klimatikus hatások szerepe a magaspartok fejlődésében (Role of climatic effects in the development of high banks). Földtani Kutatás XXXVI, 14–20 (in Hungarian).

Karácsonyi, S., Scheuer, Gy., 1972. A dunai magaspartok építésföldtani problémái (Engineering geological problems of high banks along the Danube). Földtani Kutatás 15, 71–83 (in Hungarian with Russian abstract).

Karbon, M., Brückl, E., Hegedűs, E., Preh, A., 2011. Kinematics of a mass movement constrained by sparse and inhomogeneous data. Natural Hazards and Earth System Sciences 11, 1609–1618.

Kaszás, F., Kraft, J., 2009. A dunaszekcsői magaspart rogyásos suvadása (Slumping of the bank at Dunaszekcső). Mélyépítő Tükörkép Magazin 8, 35–39 (in Hungarian).

Kézdi, Á., 1970. A dunaújvárosi partrogyás (The bank collapse at Dunaújváros). Mélyépítéstudományi Szemle 20, 281–297 (in Hungarian).

Kleb, B., Schweitzer, F., 2001. A Duna csuszamlásveszélyes magaspartjainak településkörnyezeti hatásvizsgálata (Assessment of the impact of landslide prone high banks on urban environment along the River Danube). In: Ádám, A., Meskó, A. (Eds.), Földtudományok és a földi folyamatok kockázati tényezői. Bp. MTA, pp. 169–193 (in Hungarian).

Kraft, J., 2005. A dunaszekcsői Töröklyuk kialakulása és fennmaradása (Evolution and survival of the Töröklyuk cave at Dunaszekcső). Mecsek Egyesület Évkönyve a 2004–es egyesületi évről. Új Évfolyam, vol. 8, pp. 133–153 (in Hungarian).

Kraft, J., 2011. Dunai magaspart dunaszekcsői részletének rogyásos suvadásai (Slumping of Danube's high bank at Dunaszekcső). In: Török, Á., Vásárhelyi, B. (Eds.), Mérnökgeológia–Kőzetmechanika 2011, pp 1–12 (in Hungarian).

Lóczy, D., Balogh, J., Ringer, Á., 1989. Landslide hazard induced by river undercutting along the Danube. In: Embleton, C., Federici, P. R., Rodolfi, G. (Eds.), Geomorphological Hazards, Supplements of Geografia Fisica e Dinamica Quaternaria, 2, 5–11.

Lóczy, D., Kertész, Á., Lóki, J., Kiss, T., Rózsa, P., Sipos, Gy., Sütő, L., Szabó, J., Veress, M., 2012. Recent Landform Evolution in Hungary. In: Lóczy, D., Stankoviansky, M., Kotarba, A., (Eds.), Recent Landform Evolution – The Carpatho–Balkan–Dinaric Region, Series: Springer Geography (2). Springer Science+Business Media BV, Heidelberg – London – New York, 205–247.

Mentes, Gy., Bányai, L., Újvári, G., Papp, G., Gribovszki, K., Bódis, V.B., 2012. Recurring mass movements on the Danube's bank at Dunaszekcső (Hungary) observed by geodetic methods. Journal of Applied Geodesy 6, 203– 208.

Moyzes, A., Scheuer, Gy., 1978. A dunaszekcsői magaspart mérnökgeológiai vizsgálata (Engineering geological investigation of the high bank at Dunaszekcső). Földtani Közlöny 108, 213–226 (in Hungarian with German abstract).

Papp, G., 2009. Simultaneous determination of terrain correction and local average topographic density. Acta Geodaetica and Geophysica Hungarica 44, 191– 202.

Pécsi, M., Scheuer, Gy., 1979. Engineering geological problems of the Dunaújváros loess bluff. Acta Geologica Hungarica 22, 345–353.

Pécsi, M., Schweitzer, F., Scheuer, Gy., 1979. Engineering geological and geomorphological investigations of landslides in the loess bluffs along the Danube in the Great Hungarian Plain. Acta Geologica Hungarica 22, 327–343.

Rinaldi, M., Casagli, N.,1999. Stability of streambanks formed in partially saturated soils and effects of negative pore water pressures: the Sieve River /Italy/. Geomorphology 6, 253–277.

Rónai, A., 1985. The Quaternary of the Great Hungarian Plain. In: Pécsi, M. (Ed.), Loess and the Quaternary. Akadémiai Kiadó, Budapest, pp. 51–63.

Scheuer, Gy., 1979. A dunai magaspartok mérnökgeológiai vizsgálata (Engineering geological investigation of the high banks of the Danube). Földtani Közlöny 109, 230–254 (in Hungarian with German abstract).

Simon, A., Curini, A., Darby, S.E., Langendoen, E.J., 2000. Bank and near–bank processes in an incised channel. Geomorphology 35, 193–217.

Strang, G., Borre, K., 1997. Linear Algebra, Geodesy, and GPS. Wellesley–Cambridge Press

Szabó, J., 2003. The relationship between landslide activity and weather: examples from Hungary. Natural Hazards and Earth System Sciences 3, 43–52.

Szederkényi, T., 1964. A baranyai Duna menti mezozoós szigetrögök földtani viszonyai (Geological conditions of the Mesozoic blocks along the River Danube in county Baranya). Földtani Közlöny 94, 27–32 (in Hungarian with German abstract).

Teunissen, P. J. G., 2001. Dynamic Data Processing – Recursive Least–squares. Series on Mathematical Geodesy and Positioning. Delft Universite Press, Delft, The Nederlends

Újvári, G., Mentes, Gy., Bányai, L., Kraft, J., Gyimóthy, A., Kovács, J., 2009. Evolution of a bank failure along the River Danube at Dunaszekcső, Hungary. Geomorphology 109, 197–209.

Urbancsek, J., 1977. Magyarország mélyfúrású kútjainak katasztere VII. Cadastre of the deep–drilling wells in Hungary VII, p. 268 (in Hungarian).

Závoti, J., 2012. A simple proof of the solutions of the Helmert and the overdetermined nonlinear 7–parameter datum transformation. Acta Geod. Geoph. Hung., 47, 453–464.